Buckling of Glass-Reinforced Plastic Cylindrical Shells Under Combined Axial Compression and External Pressure

Ghazi A. F. R. Abu-Farsakh* and J. K. Lusher†
University of London, London, England, U.K.

The paper describes the results of a theoretical and experimental investigation into the buckling behavior of glass-reinforced plastic cylindrical shells under the action of combined axial load and internal pressure. A total of 20 shells were loaded to buckling. Initial imperfections, load-deflection response, and buckling modes and loads were determined experimentally and compared with the results of a finite element analysis. This analysis utilized a buckling criterion developed on the basis of the total potential energy. The proposed method of buckling load prediction is shown to give close agreement with the experimental results.

Nomenclature

Ax	= variable axial compression load
Ax_{ex}	= experimental axial compression buckling load
Ax_{im}	= imperfect axial compression buckling load
Ax_{pr}	= perfect axial compression buckling load
C	= constant coefficient
DR^+	= incremental potential energy of internal forces
g_0^+	= incremental applied loads
g_i^+	= out-of-balance forces or gradient ($i=0$)
i	= iteration number
$[K_T]$	= structure tangential stiffness matrix at the beginning of each increment
p	= variable external pressure load
SINC_ℓ	= size of initial load increment
SINC_i	= size of load increment i
SR^+, SRI^+	= incremental potential energies of applied loads and out-of-balance forces, respectively
V_{im}	= variable imperfect load
V_{pr}	= variable perfect load
$\{W_s\}$	= total structure displacement vector
$\{\gamma\}$	= force vector defined by Eq. (2)
Δ	= increment
δ	= variation
Π	= total structure potential energy
$\{\ \}, \lfloor\ \rfloor$	= column and row vectors, respectively
$[\ ]$	= rectangular or square matrix
$(\ )^+$	= opposite sign to that usually adopted

Introduction

CONSIDERABLE research effort has been directed in recent years to the study of the influence of initial imperfections on the buckling of cylindrical shells. There is a general agreement between investigators that initial imperfections and boundary conditions are the major cause of disagreement between theoretical and experimental buckling loads. Moreover, geometrical imperfections having the shape of the natural buckling mode have the most marked effect on the reduction of the critical load. Some investigators include this effect by adding a constantly changing displacement mode. Others have adopted a general random shape imperfection distribution.[1] The influence of the initial imperfections depends on the shape of the secondary equilibrium path for the corresponding perfect structure. Hence, if the path curves downward, the equilibrium is unstable on the secondary path, the buckling is abrupt, and the buckling load of the imperfect structure is reduced. On the other hand, if the path curves upward, the structure may have considerable postbuckling strength,[2] as will be observed later in this paper in the case of the group I cylinders.

The objectives of this paper are:

1) To show the effect of initial geometrical imperfections on the buckling of glass-reinforced plastic (GRP) cylindrical shells (the other type of initial imperfections is due to nonuniform axial load distribution and is explained in Ref. 6).

2) To show the effectiveness and importance of the proposed buckling criterion in reducing the critical load.

Derivation of Buckling Criterion

A buckling criterion is suggested that utilizes a formula involving the incremental total potential energy function $\Delta\Pi$. In the case of a quadratic governing function $\Delta\Pi$ is given by Ref. 3 as

$$\Delta\Pi_i = \lfloor \delta W_s \rfloor_i \{g\}_i + \tfrac{1}{2} \lfloor \delta W_s \rfloor_i [K_T] \{\delta W_s\}_i \tag{1}$$

where i indicates the iteration number.

By introducing the equilibrium equation

$$\{\gamma\}_{i+1} = [K_T] \{\delta W_s\}_i \tag{2}$$

and substituting in Eq. (1), we obtain

$$\Delta\Pi_i = \lfloor \delta W_s \rfloor_i \{g\}_i + \tfrac{1}{2} \lfloor \delta W_s \rfloor_i \{\gamma\}_{i+1} \tag{3}$$

For the sake of simplicity of notation, let us assume

$$SR = \lfloor \delta W_s \rfloor_i \{g\}_i \tag{4}$$

$$SRI = \lfloor \delta W_s \rfloor_i \{g\}_{i+1} \tag{5}$$

$$DR = SRI - SR = \lfloor \delta W_s \rfloor_i \{\gamma\}_{i+1} \tag{6}$$

Then, substituting these relations in Eq. (3) yields

$$\Delta\Pi_i = SRI - \tfrac{1}{2} DR \tag{7}$$

At buckling, $\Delta\Pi_i$ becomes equal to zero. Hence,

$$SRI - \tfrac{1}{2} DR = 0 \tag{8}$$

Consequently, for a stable system the increment $\Delta\Pi_i$ must always be less than zero (the negative sign of $\Delta\Pi_i$ is due to the negative sign of $\{g\}_i$), i.e., $\Delta\Pi_i < 0$ so that

$$SRI/DR < 0.5 \tag{9}$$

Received March 30, 1984.

*Research Student, Department of Civil Engineering, Queen Mary College; currently Assistant Professor of Civil Engineering, Yarmouk University, Jordan.

†Lecturer, Department of Civil Engineering, Queen Mary College.

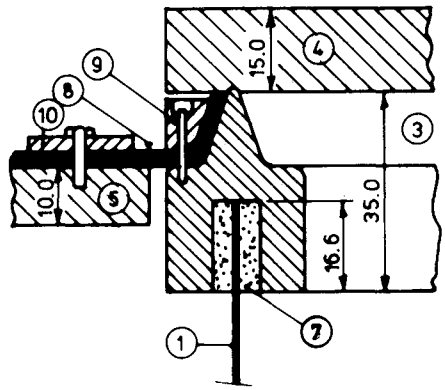

Fig. 1a Cross section showing top end fixity.

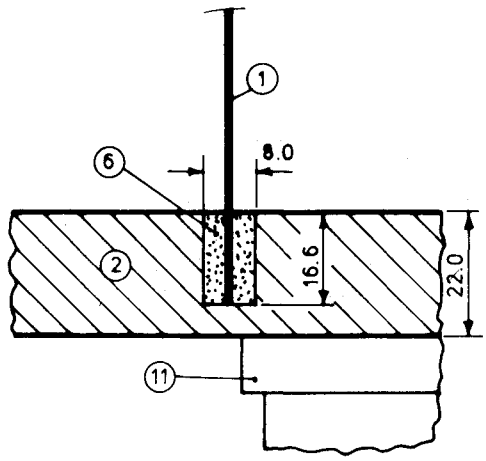

Fig. 1b Cross section showing bottom end fixity.

Accordingly, for an unstable system the increment $\Delta\Pi_i$ is always greater than zero, i.e.,

$$\Delta\Pi_i > 0 \tag{10}$$

This criterion can be easily incorporated in a finite element incremental nonlinear program so as to detect the critical load.

Experimental Study

Test Specimens

The test specimens used were cylindrical shells made of a glass-reinforced plastic-type woven roving (WR) cloth (warp:weft = 1:1) embedded in heat-resistant polyester resin.

Twenty test specimens were studied. The specimens were divided into four groups according to their L/d ratios, which were 0.5-2. The nominal diameters and thicknesses of each group were the same ($d = 305.30$ mm, $t = 1.00$ mm). The shell walls were of a composite construction consisting of three layers of equal nominal fiber thicknesses (0.30 mm each), each having the same fiber orientations.

Mounting Procedure and Instrumentation

Figure 1 shows the test fixture. Each cylindrical shell (1) was mounted on the circular steel base plate (2) with the bottom edge lying in the circular groove (6), which had been machined into the plate. The top edge of the cylinder was lying in another circular groove (7) in the steel ring (3).

Both the top and bottom grooves were filled with the low-melting-point (70°C) alloy (MCP-70) to provide end fixity. Two circular heating plates were fixed under the base plate (their centers aligned symmetrically on the same diameter) so as to melt the alloy.

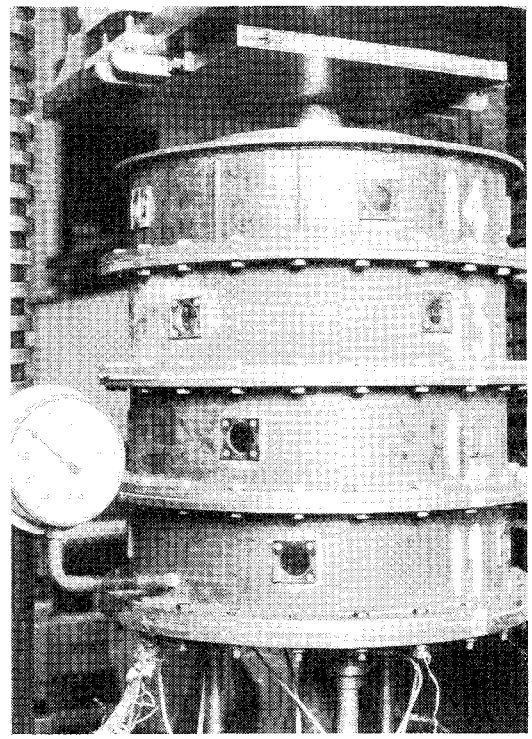

Fig. 2 Pressure test rig (as used for group IV cylinders).

The test rig (Fig. 2) consisted of four steel cylinders (used in four stages according to cylinder length) that enclosed the space around the test specimen. A diaphragm pump (Edwards High Vacuum, model D1) was used to provide the external air pressure. This air pressure was controlled during the experiment with the aid of a Manostat control valve (John Watson and Smith Ltd., type MR3/1/SR/240V). The pressure was measured using a pressure transducer (RDP Electronics Ltd., type P5/50) together with a mechanical pressure gage that checked the pressure inside the test rig.

The axial compression loading was applied by a Mohr and Federhaff testing machine. To ensure, as far as possible, the symmetry and uniformity of application of the axial load, a solid stainless steel ball (diameter 76.00 mm) was placed in the center of the top steel plate. In addition, three load cells on the top of three screw jacks were placed under the bottom steel plate.

Two displacement transducers were placed on a central stainless steel tube (25.00 mm o.d. machined to a very high accuracy) so as to measure geometrical imperfections on both sides of the cylinder. Radial deformations were measured during the experiment at the top and midheight of each specimen.

A stepper motor (1.8 deg/step) was used in double steps to rotate the central shaft. For each cylinder, the load was plotted against the deflection at a point of expected maximum deflection at midheight.

Examples of the buckled cylinders are shown in Figs. 3 and 4.

Theoretical Analysis

A nonlinear analysis program NONL5 utilizing the finite element method was developed. The elements were triangular (10 nodes/element) and all displacement functions were complete cubic polynomials.[6] In the analysis, Sanders' nonlinear strain displacement relationships,[4] which account for large deformations and moderate rotations, were adopted. The analysis is based on an incremental technique using the accelerated modified Newton-Raphson method.[3,5]

The radial geometrical imperfections are introduced at the corner and midside nodes of the finite element mesh (a 6×6

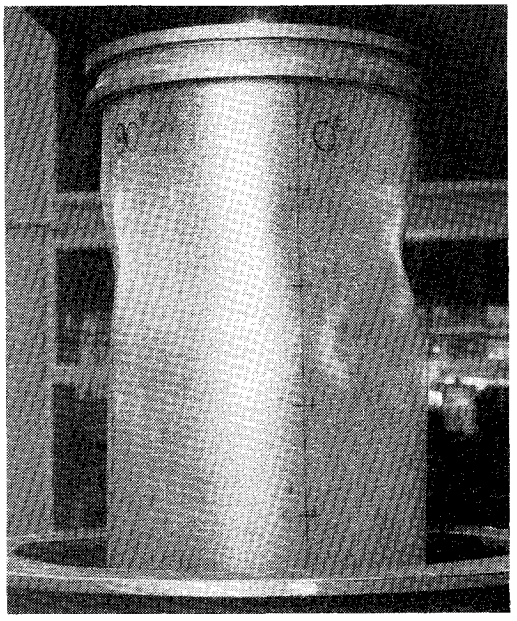

Fig. 3 Cylinder 1/IV in postbuckled state at 0 deg.

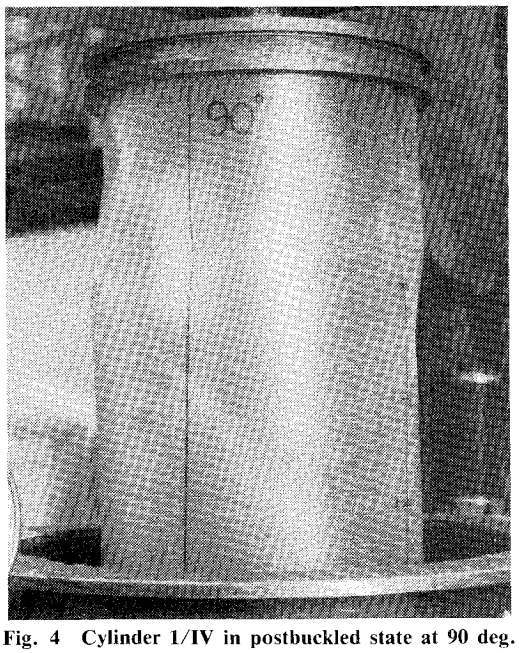

Fig. 4 Cylinder 1/IV in postbuckled state at 90 deg.

mesh forming 72 triangular elements). The imperfection distribution is assumed to have a quadratic variation across the element.

In order to simulate the experimental behavior of the load-deflection path of the combined loading case, in the theoretical analysis the constant load (either axial compression or external pressure) is first applied until the total load equals the corresponding experimental value. Then, increments of the variable load are applied until buckling is reached.

The size of the new load increment is generated in accordance with

$$\mathrm{SINC}_i = (1 + SRI/DR)_{i-1}\mathrm{SINC}_{i-1} \tag{11}$$

where i is the increment number.

A suitable initial size of the load increment may be assumed according to

$$\mathrm{SINC}_\ell = C \times \text{critical load} \tag{12}$$

Table 1 Cylinders geometric and material properties

Cylinder no.	R, mm	L_{total}, mm	L_{net}, mm	t_{av}, mm	E_{av}, N/mm^2	ν_{av}
1/I	153.46	151.42	121.5	0.927		
2/I	153.01	153.29	117.8	0.968		
3/I	153.02	152.88	117.95	0.928	16,866	0.168
4/I	153.51	153.13	119.40	0.987		
5/I	153.94	152.00	118.25	0.869		
1/II	153.47	304.51	273.01	0.881		
2/II	153.24	305.35	272.90	0.947		
3/II	153.22	305.23	272.23	0.947	15,483	0.172
4/II	153.07	304.22	272.88	0.862		
5/II	153.52	305.08	273.25	0.890		
1/III	153.31	458.25	424.00	0.935		
2/III	152.77	456.88	427.63	0.946		
3/III	153.20	457.00	424.00	0.974	16,651	0.175
4/III	153.54	457.25	425.00	0.978		
5/III	153.42	457.38	423.75	0.952		
1/IV	153.45	610.63	576.38	0.935		
2/IV	153.58	608.88	576.63	1.000		
3/IV	153.09	609.00	576.50	0.967	17,081	0.166
4/IV	153.65	609.50	577.56	0.987		
5/IV	154.03	609.63	576.00	0.987		

where $C = 0.1$ in the case of axial compression and 0.2 in the case of pressure.

Smaller load increments are needed in the vicinity of the critical load and a reanalysis at the current increment (e.g., halving the size of the increment) is necessary (see Sec. 5.2.3 of Ref. 6).

Results and Discussion

The actual dimensions of the cylinders are shown in Table 1. Comparisons between experiment and theory are shown in Tables 2-4. The buckling modes of two cylinders are shown in Figs. 5 and 6.

During the analysis, the ratio SRI/DR was always kept greater than or equal to -1 and less than or equal to 0.5 in order to satisfy the buckling criterion, i.e.,

$$-1 \le (SRI/DR) \le 0.50 \tag{13}$$

In many cases, the positive ratio was found to be increasing until the buckling point was reached, except for very small values of the ratio, i.e.,

$$(SRI/DR) < 0.005 \qquad \text{(for a } 6\times 6 \text{ mesh)} \tag{14}$$

For more details, see Sec. 5.2.3 of Ref. 6. (Reference 6 includes an intensive survey of the behavior of the ratio SRI/DR for several cylinders, both perfect and imperfect.)

The results in Tables 2-4 and Figs. 7-9 show the close agreement between the experimental and theoretical results that invariably satisfied Eqs. (13) and (14). This conclusion is also supported, to some extent, by the similarity in the load-deflection results in which the maximum detected deflections for both experiment and theory were in good agreement (Figs. 7 and 8).

The load-deflection curve for cylinder 5/I (see Fig. 9) exhibited stiffening behavior after buckling (all of the cylinders of group I exhibited this behavior, except those under axial compression load only, see Table 2).

In analyzing the cylinders of groups III and IV, only half of a cylinder is considered using a 6×6 mesh and the imperfections were introduced as explained earlier. On the other hand, the cylinders of groups I and II, in general, exhibited higher circumferential buckling modes (i.e., $n > 6$, where n is the number of critical circumferential waves). Thus, in order to achieve a more accurate representation, a

Table 2 Comparison between experimental and theoretical buckling loads for cylinders of groups I and II, uniform axial load distribution

Cylinder no.	Load case	Variable load	Experimental results		Results from finite element program NONL5					
			Ax_{ex}, kN	p_{ex}, N/mm^2	Ax_{im}, kN	p_{im}, N/mm^2	Ax_{pr}, kN	p_{pr}, N/mm^2	V_{ex}/V_{im}	V_{ex}/V_{pr}
1/I	1	p	00.000	0.08816 (10)[a]	—[b]	0.08764 (12)[a]	—[b]	0.08807	1.006	1.001
2/I	1	Ax	43.126	0.00000	30.453 43.486[c]	—[b]	64.784	—[b]	1.416 0.992	0.676 —
3/I	2	Ax	41.187	0.00000	42.507 (12)[a]	—[b]	60.800	—[b]	0.969	0.666
4/I	1	Ax	10.000	0.08779	—[d]	—[d]	—[d]	—[d]	—	—
5/I	1	p	00.000	0.08167 (11)[a]	—[b]	0.08589 (12)[a]	—[b]	0.08922	0.951	0.915
1/II	1	Ax	37.638	0.00000	39.658	—[b]	57.373	—[b]	0.949	0.656
2/II	1	p	00.000	0.04417 (7)[a]	—[d]	0.03641 (8)[a]	—[b]	0.03504 0.04412[+]	1.213 —	1.248 1.074
2/II	2	p	9.331	0.03268	—[d]	—[d]	—[b]	0.03293	—	0.992
3/II	1	p	9.960	0.03618 (6)[a]	—[d]	—[d]	—[b]	0.03185	—	1.136
3/II	2	p	12.922	0.03367	—[d]	—[d]	—[b]	0.03048	—	1.105
3/II	3	p	18.413	0.02767	—[d]	—[d]	—[d]	0.02789	—	0.992
4/II	1	Ax	35.304	0.01365	26.720 37.748[c]	—[b]	36.399 53.630[c]	—[b]	1.321 0.935	0.970 0.658
5/II	1	p	33.489	0.01547	—[d]	—[d]	—[b]	0.01627	—	0.951
5/II	2	p	20.269	0.02936	—[d]	—[d]	—[b]	0.02363	—	1.242

[a]Number of circumferential waves in the buckle pattern at station 3. [b]A constant load equal to the corresponding experimental load. [c]Analysis of half a cylinder; nonuniform axial load intensity is 0.96-1.10. [d]Result not considered.

Table 3 Comparison between experimental and theoretical buckling loads for cylinders of group III, nonuniform axial load intensity 0.97-1.00

Cylinder no.	Load case	Variable load	Experimental results		Results from finite element program NONL5					
			Ax_{ex}, kN	p_{ex}, N/mm^2	Ax_{im}, kN	p_{im}, N/mm^2	Ax_{pr}, kN	p_{pr}, N/mm^2	V_{ex}/V_{im}	V_{ex}/V_{pr}
1/III	1	Ax	41.884 (5)[a]	0.00000	45.140[b] (5)[a]	—[c]	52.317[b]	—[c]	0.928	0.801
2/III	1	p	00.000	0.03135 (6)[a]	—[c]	0.02994 (6)[a]	—[c]	0.03292	1.047	0.952
3/III	1	p	10.560	0.02431	—[c]	0.02861 (7)[a]	—[c]	0.03121	0.850	0.779
3/III	2	p	20.387	0.01897	—[c]	0.02342 (5)[a]	—[c]	0.0275	0.810	0.690
4/III	1	p	24.644	0.02781 (5)[a]	—[c]	0.02958 (5)[a]	—[c]	0.02680	0.940	1.037
5/III	1	p	29.615	0.02149	—[c]	0.02116 (5)[a]	—[c]	0.02332	1.016	0.992

[a]Number of circumferential waves in the buckle pattern at station 3. [b]Nonuniform axial intensity is 0.96-1.10. [c]A constant load equal to the corresponding experimental load.

Table 4 Comparison between experimental and theoretical buckling loads for cylinders of group IV, uniform axial load distribution

Cylinder no.	Load case	Variable load	Experimental results		Results from finite element program NONL5					
			Ax_{ex}, kN	p_{ex}, N/mm^2	Ax_{im}, kN	p_{im}, N/mm^2	Ax_{pr}, kN	p_{pr}, N/mm^2	V_{ex}/V_{im}	V_{ex}/V_{pr}
1/VI	1	Ax	47.612	0.00000	45.080 (5)[a]	—[b]	48.437	—[b]	1.056	0.983
2/IV	1	p	00.000	0.02958 (5)[a]	—[b]	0.02585 (5)[a] 0.03226[c]	—[b]	0.02754 0.03314[c]	1.144 0.917	1.074 0.893
3/IV	1	p	13.861	0.02336	—[b]	0.02054 (5)[a]	—[b]	0.02124	1.137	1.100
3/IV	2	Ax	10.444	0.02403	—[d]	—[d]	7.571	—[b]	—	1.379
4/IV	1	Ax	35.520 (5)[a]	0.01838	30.650 (5)[a]	—[b]	32.227	—[b]	1.159	1.102
5/IV	1	p	21.086	0.02412	—[b]	0.02346 (5)[a]	—[b]	0.02160	1.028	1.117

[a]Number of circumferential waves in the buckle pattern at station 3. [b]A constant load equal to the corresponding experimental load. [c]Axial displacement fixed at top end. [d]Result not considered.

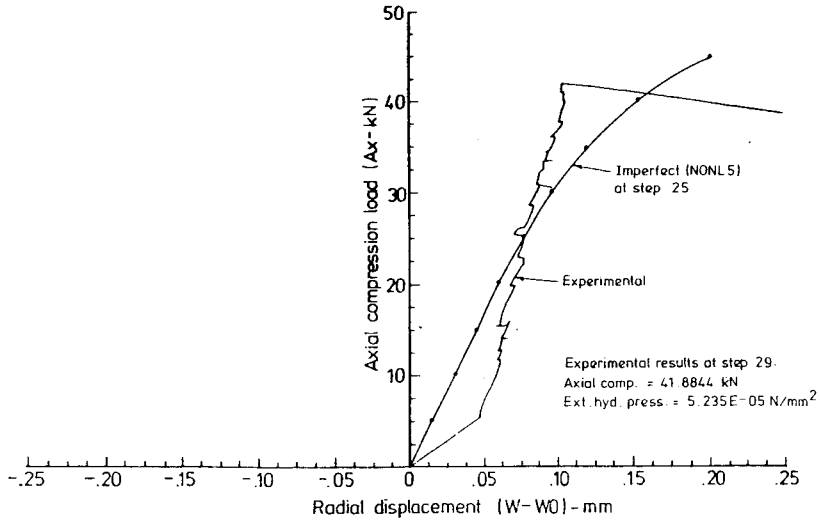

Fig. 5 Buckling mode for cylinder 1/III.

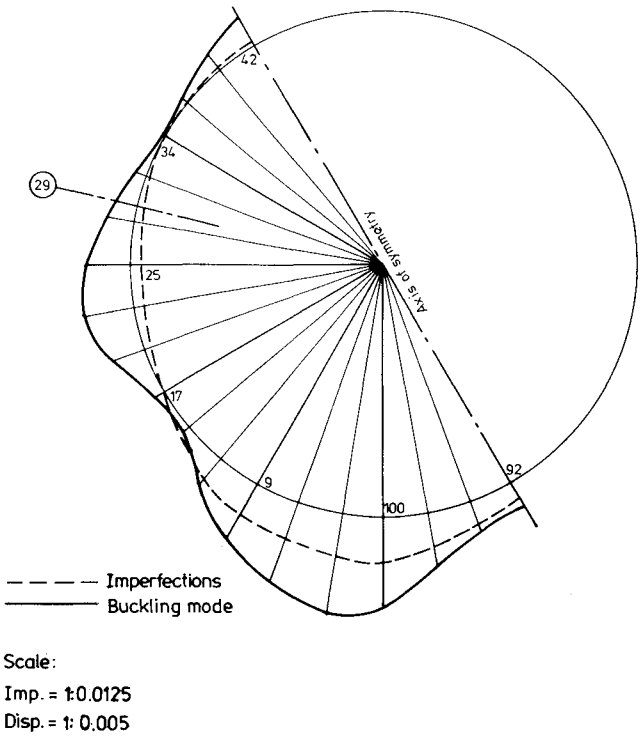

Fig. 6 Buckling mode for cylinder 5/IV.

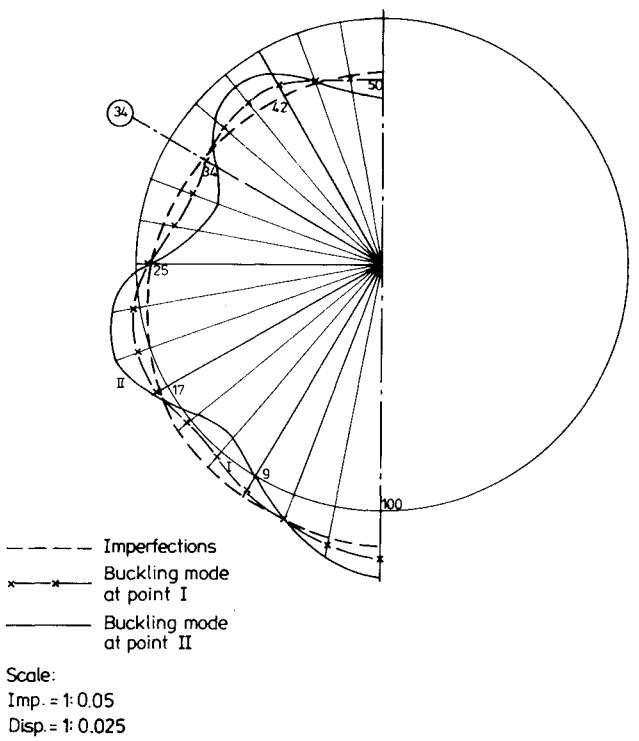

Fig. 8 Load-deflection curves for cylinder 5/IV.

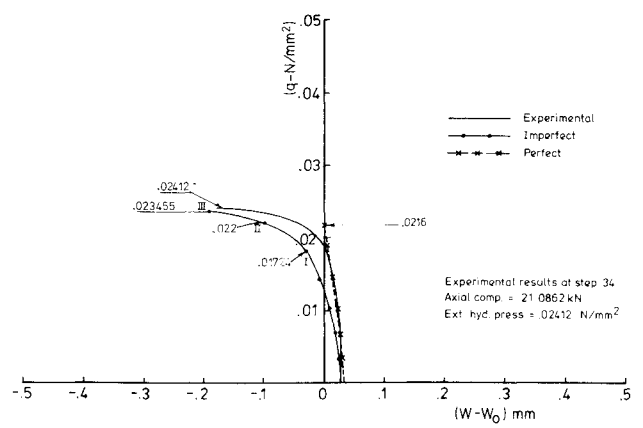

Fig. 7 Load-deflection curves for cylinder 1/III.

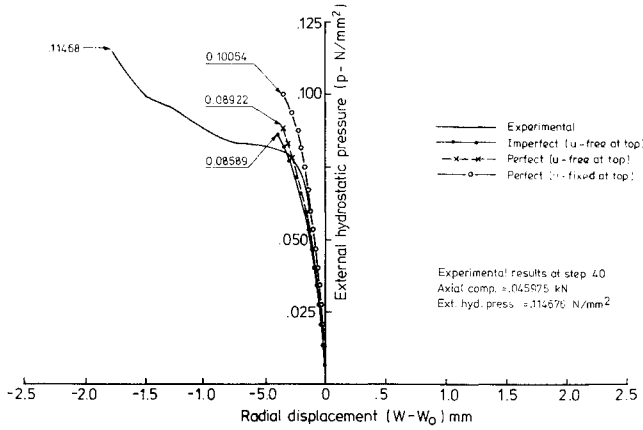

Fig. 9 Load-deflection curves for cylinder 5/I.

quarter of a cylinder was analyzed using the same mesh pattern. In this case, as an approximation, the geometrical imperfections were assumed to have the same distribution as that of half a cylinder. In most cases, this approximation led to unreasonable buckling loads for the group II cylinders (because the imperfections were mainly designed to fit half a cylinder), except those of cylinders 1/II and 2-3/I. For group II cylinders, only the perfect buckling loads are considered, except that of cylinder 1/II.

General Conclusions

From the experimental and theoretical results, the following conclusions can be drawn:

1) The agreement between the experimental and theoretical results is close, between $\pm 15\%$.

2) Repeated loading (for loads up to the buckling load) has some effect on reducing the experimental buckling loads depending upon whether or not a cylinder has undergone any plastic deformation.

3) The effect of initial geometrical imperfections in reducing the buckling loads of cylindrical shells under axial compression is a major factor (in some cases, this could be about 30%). On the other hand, buckling loads of cylindrical shells under external pressure are less affected (in some cases, the action may be reversed, see Tables 2-4). The shape of these imperfections plays an important part in reducing the buckling load, particularly when such imperfections have the form of the buckling mode. The effect of initial geometrical imperfections is very small when the postbuckling behavior is stiffening.

4) In general, the finite element method for analyzing cylindrical shells under external pressure predicts lower theoretical buckling loads than the experimental ones. This conclusion was also reached in Ref. 7.

5) The size of the finite element mesh is very important, especially when the number of circumferential waves is higher than the number of divisions in that direction. (When half a cylinder was used in analyzing cylinders of group II, the resulting buckling loads were, in some cases, as high as 40% of those using a quarter of a cylinder, e.g., most of the cylinders of group II.)

References

[1]Abi-Shaheen, S. A., "Buckling of Composite Shells of Revolution," Ph.D. Thesis, Queen Mary College, University of London, London, Feb. 1979.

[2]Brush, D. O. and Almroth, B. O., *Buckling of Bars, Plates and Shells*, McGraw-Hill Book Co., New York, 1975.

[3]Crisfield, M. A., "Iterative Solution Procedures for Linear and Nonlinear Structural Analysis," Dept. of the Environment, Transport and Road Research Laboratory, Crowthorne, Rept. TRRL-LR-900, 1979.

[4]Brebbia, C. A. and Connor, J. J., *Fundamentals of Finite Element Techniques for Structural Engineers*, Butterworths, London, 1973.

[5]Crisfield, M. A., "Large-Deflection Elasto-Plastic Buckling Analysis of Plates Using Finite Elements," Dept. of the Environment, TRRL, Crowthorne, Rept. TRRL-LR-593, 1973.

[6]Abu-Farsakh, G. A., "Analytical and Experimental Study of Buckling of Composite Shells," Ph.D. Thesis, Queen Mary College, University of London, London, Dec. 1983.

[7]Tennyson, R. C., "The Effect of Shape Imperfections and Stiffening on the Buckling of Circular Cylinders," *Conference on Buckling of Structures Symposium*, (IUTAM Symposium), Cambridge, MA, June 1974, pp. 251-273.